Wrinkle Morphology Effects on Thermoelastic Spring-In in Composite L-Sections

Connor Long[1*], Yuping Tao[2], and Anoush Poursartip[1]

[1]Composites Research Network, Department of Materials Engineering, The University of British Columbia, Vancouver, Canada, [2]Boeing, USA

* *Connor Long (connor.long@composites.ubc.ca)*

Keywords: *Process-Induced Deformation; Composites; Spring-in; Modelling; Wrinkling*

1. Abstract

The manufacturing of composite structures to aerospace tolerances requires compensation for process-induced deformations such as spring-in and warpage. Currently, typical process models assume smooth geometry and uniform plies. This paper presents an automated 2D finite element workflow applied to a quasi-isotropic 64-ply L-shaped composite to study how prescribed wrinkle morphologies influence thermoelastic spring-in and flange warpage. For a smooth IML convex L-section, a single wrinkle with varying severity L/d, depth, and attenuation was modelled to assess their effects on spring-in and warpage. The results demonstrate that wrinkle morphology should be included as a spatial geometric input in process-induced deformation models to improve dimensional prediction accuracy.

2. Introduction

Composite materials are used in aerospace for their high specific stiffness and strength, but the processed parts must also meet tight dimensional tolerances. Process-induced deformation (PID) — often manifesting as corner spring-in or flange warpage (Figure 1) — can cause assembly gaps, requiring shimming or forced assembly (within allowed limits) [1]. Spring-in in curved composite laminates arises from anisotropic free-strain mismatch between the in-plane and through-thickness directions. Following Radford and Rennick [2], the thermal and cure-shrinkage contributions to spring-in may be written as

$$\Delta\theta = \Delta\theta_{CTE} + \Delta\theta_{CS} = \theta\left(\frac{(CTE_l - CTE_t)\Delta T}{1 + CTE_t\Delta T}\right) + \theta\left(\frac{\phi_l - \phi_t}{1 + \phi_t}\right) \tag{1}$$

showing that directional free-strain mismatch drives spring-in. This formulation and the more sophisticated Finite Element Modelling (FEM) predictions, however, typically omit local manufacturing deviations—such as geometry changes, fibre orientation/thickness variations, resin redistribution, voids, waviness, and wrinkles—that occur at corners during lay-up, debulking, and consolidation [3]. In manufactured L-sections, spring-in is typically on the order of 1–1.5°, but this introductory and preliminary study focuses on the cooldown thermoelastic-reversible component of corner spring-in, ignoring cure shrinkage for simplicity. We note that most experimental and numerical studies on wrinkles have focused on stiffness and strength reductions [4-6].

Previous work by Çınar and Ersoy found that wrinkling in thin L-laminates reduced spring-in [7], prompting the modelling question: which wrinkle features control changes in spring-in, and when do they matter? The present work develops an automated finite-element workflow applied to a 64-ply quasi-isotropic L-section (Figure 2) to quantify thermoelastic PID from prescribed, cured-in wrinkle geometry, characterized by depth, wavelength, defect-zone width, through-thickness attenuation, originating interface, and location, and tracked by the wavelength-to-depth ratio L/d, while holding material properties constant to isolate geometric effects.

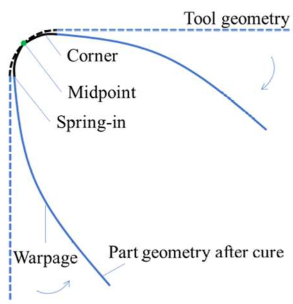

Figure 1. Schematic illustration of PID modes in an L-section laminate [8].

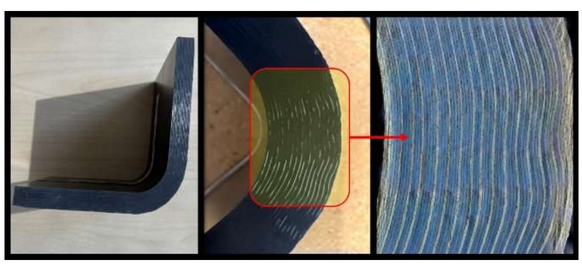

Figure 2. Observed typical corner waviness in a 64-ply composite L-section sample.

3. Model Scope and Wrinkle Definition

3.1. Model scope

The nominal L-section geometry, boundary conditions, and fibre-direction convention are shown in Figure 3. The nominal model is a 2D L-section with a 20 mm inner radius, a 68.096 mm flange length, a 90° initial included angle, and a smooth IML tool-side condition. The laminate is a 64-ply $[-45/0/45/90]_{8s}$ layup, with a nominal ply thickness of 0.190 mm and a nominal laminate thickness of 12.16 mm. Each ply is assigned orthotropic elastic lamina properties with E_1= 148 GPa, $E_2 = E_3 = 10.1$ GPa, $G_{12} = G_{13} = 3.94$ GPa, $G_{23} = 3.48$ GPa, $\alpha_{11} = 0.60 \times 10^{-6}$ °C^{-1}, and $\alpha_{22} = \alpha_{33} = 28.6 \times 10^{-6}$ °C^{-1}. A uniform cooldown from 180 °C to 20 °C is applied. The model does not simulate wrinkle formation during cure; instead, wrinkles are prescribed as cured-in geometric features and compared to a smooth L-section under cooldown-only thermoelastic loading, isolating geometric effects from cure-dependent property changes, resin flow, and cure shrinkage. Wrinkled models are created by defining ply interfaces in a local coordinate system, allowing variation of depth, wavelength, through-thickness location, attenuation, and IML/OML smoothing. Local ply thickness may change, but lamina properties remain constant and follow the lamina path for each ply. Thus, this study is a constant-property sensitivity analysis of wrinkle morphology rather than a resin-redistribution model.

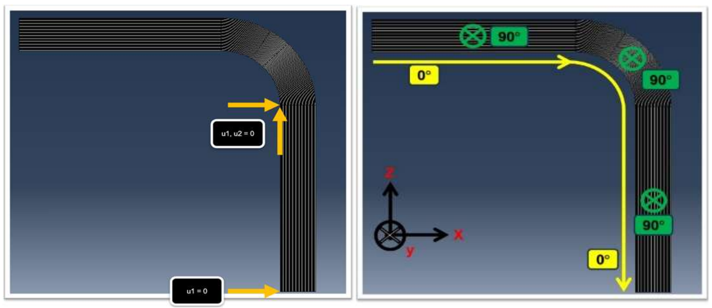

Figure 3. Nominal L-section FE model: boundary-condition and fibre orientation setup used for the cooldown simulations.

3.2. Wrinkle parameterization and profile generation

Wrinkles are generated by prescribing ply-interface displacements along the corner/flange path using a Gaussian-modulated sinusoid, adapted from the flat-coupon work by Mukhopadhyay and Xie [4,5]. This work modifies the coordinate mapping of the wrinkle profile to wrap around a corner in an L-section. At each x, the nominal interface coordinate is shifted in z to build a spline interface; repeating through the thickness at each position produces the full wrinkled corner. The perturbed interface is written as

$$z_i(x) = it_{ply} + d\exp\left[-\frac{(i-i_0)^2}{\alpha_k^2}\right]\exp\left[-\frac{(x-x_c)^2}{w_1^2}\right]\cos\left[\frac{2\pi(x-x_c-x_1)}{L}\right] \tag{2}$$

where t_{ply} is nominal ply thickness, d the maximum wrinkle depth, L the wavelength, w_1 the Gaussian envelope modulator (defect-zone width), α_k the through-thickness attenuation factor, x_c the wrinkle centre, and x_1 a phase offset. The above parameters are demonstrated in Figure 4. The wrinkle attenuation follows a Gaussian decay, where the wrinkle depth decreases by d/e (where e is Euler's number) at α_k, so larger α_k spreads the wrinkle over more interfaces (Figure 5). i_0 The wrinkle-originating interface is visualized in Figure 6.

For the L-section, the perturbed interface points are then mapped onto the curved corner geometry using,

$$\theta(x) = \frac{\pi}{2} - \frac{x}{R_{in}} \tag{3}$$

$$r_i(x) = R_{in} + z_i(x) \tag{4}$$

$$X_i(x) = r_i(x)cos\theta(x) \tag{5}$$

$$Z_i(x) = r_i(x)sin\theta(x) \tag{6}$$

where R_{in} is the inner radius, $r_i(x)$ is the radial position of interface i, and (X_i, Z_i) are the Cartesian coordinates used to build the corner FE geometry. Lowercase $z_i(x)$ is the through-thickness interface position before mapping; uppercase $Z_i(x)$ is the vertical coordinate after mapping to the rounded corner of the L-section.

The smooth-IML convex tool condition,

$$\Delta z_0(x) = 0 \tag{7}$$

Note that, in practice, wrinkle severity is often quantified by the wavelength-to-depth ratio L/d (Figure 7) and the wrinkle depth-to-laminate-thickness ratio d/t, but these metrics alone cannot fully characterize a corner wrinkle. The proposed model, therefore, specifies wrinkle depth, wavelength, defect-zone width, through-thickness attenuation and originating interface, and surface smoothing for convex or concave layups.

L/d	Approximate severity
~60	Very Mild
~30	Mild
~20	Moderate
≤ 15	Severe / Sensitivity Case

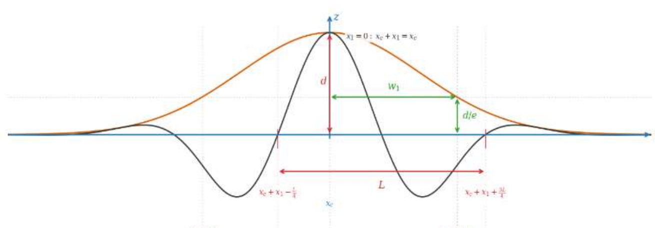

Figure 4. Prescribed wrinkle profile and geometric parameters used to define ply-interface perturbations, including wrinkle depth d, wavelength L, and defect-zone width w_1 (Adapted from [5]) with approximate wrinkle severity targets.

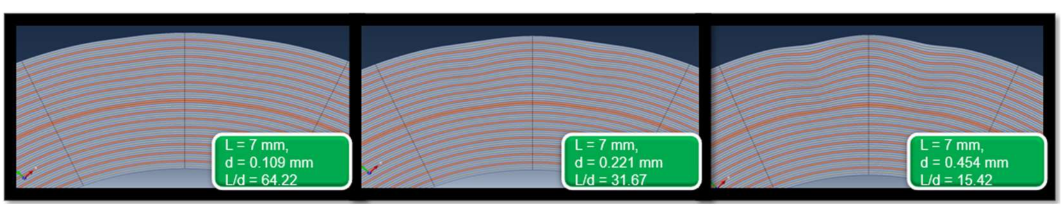

Figure 5. Wrinkle originates at ply 55, attenuation factor of 20 (i_0 = 55, α_k = 20) with very mild to moderate severities, L/d.

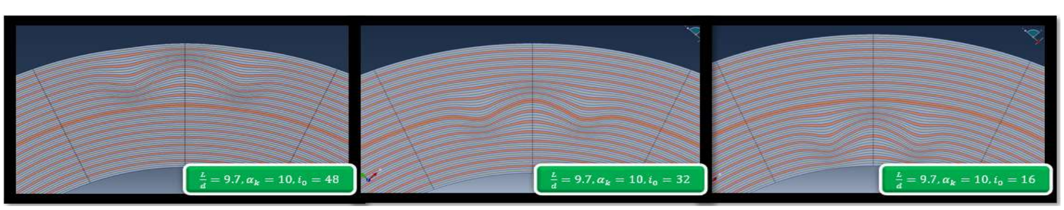

Figure 6. High severity wrinkle, attenuation factor of 10 (L/d = 9.7, α_k = 10), with varying wrinkle-originating interfaces, i_0.

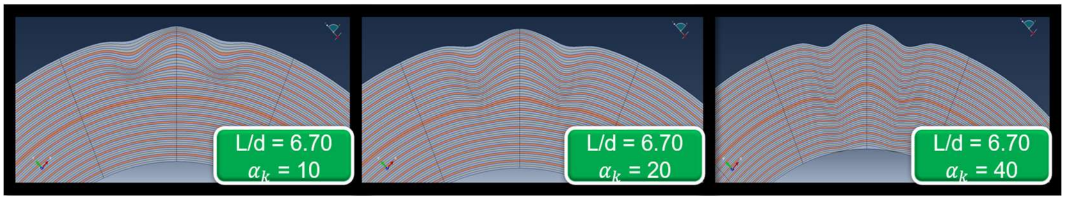

Figure 7. Very high severity wrinkle-originating at ply 55 (L/d = 6.7, $i_0 = 55$), with a narrow to broad attenuation factor, α_k.

3.3. Finite element implementation and parametric sweeps

The nominal reference is a 2D generalized plane-strain finite-element model of a smooth L-section, partitioned ply-by-ply. This study uses CPEG8 elements with an element size of approximately 0.190 mm, equivalent to t_{ply}, with pinned/roller constraints (Figure 3), and a uniform cooldown from cure to room temperature. Identical mesh, boundary conditions, thermal loading, material properties, and spring-in extraction method are used for all cases.

Models are produced by an automated Python workflow that builds ply-interface geometry, partitions the L-section, assigns sections and material orientations, applies loads and boundary conditions, meshes the model, runs the cooldown analysis, and extracts spring-in. In this paper, a single corner wrinkle morphology is considered. The parametric sweeps vary wrinkle severity L/d, wrinkle-originating interface i_0, and through-thickness attenuation factor α_k, while the nominal L-section geometry, material properties, boundary conditions, thermal loading, and extraction method are held constant. All wrinkled models are compared against the smooth nominal reference.

4. Results and Discussion

The nominal reference L-section exhibited negligible flange warpage and a maximum thermoelastic spring-in of

$$\Delta\theta_{max,nominal} = 0.47° \quad (8)$$

4.1. Effect of localized wrinkle severity

A single corner wrinkle was prescribed to originate at ply 55, with an attenuation factor of 20. As L/d decreased, corresponding to increasing wrinkle severity, the spring-in decreased. The largest changes occurred for L/d < 12. Mild wrinkles produce near-nominal spring-in values (Figure 8).

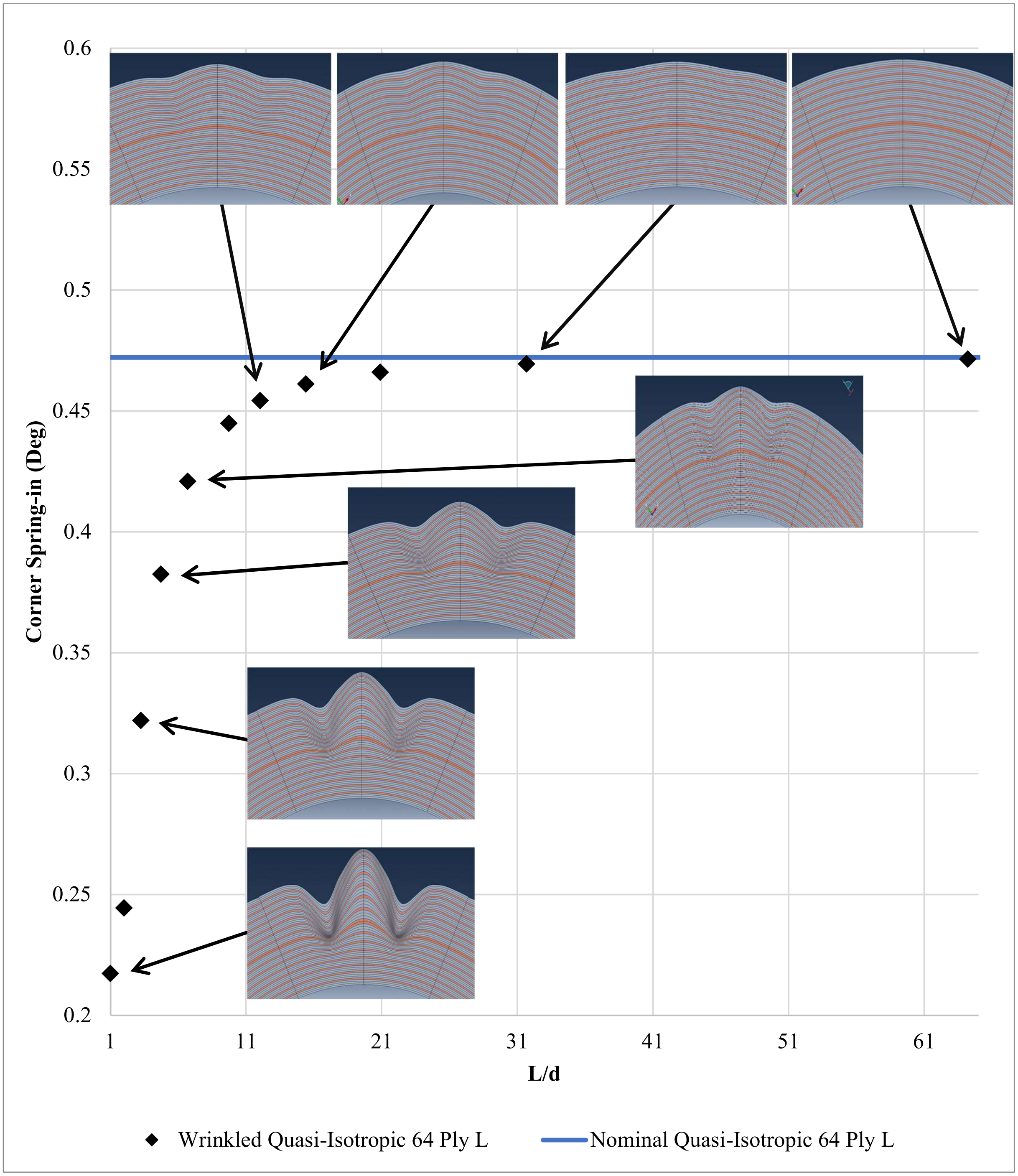

Figure 8. Effect of the severity of localized single-corner wrinkling on extracted spring-in for a 64-ply quasi-isotropic L-section; d is varied; L = 7mm, w_1 = 4mm, α_k = 20mm, smooth IML, and i_0 = 55 are held constant.

4.2. Effect of through-thickness attenuation and wrinkle location

The corner spring-in depends on both through-thickness wrinkle location and attenuation. OML-side wrinkles reduce spring-in, IML-side wrinkles increase spring-in, and midplane wrinkles (i_0 =

32) produce a smaller reduction (Figures 9 and 10). Broader attenuation amplifies these effects (Figure 10).

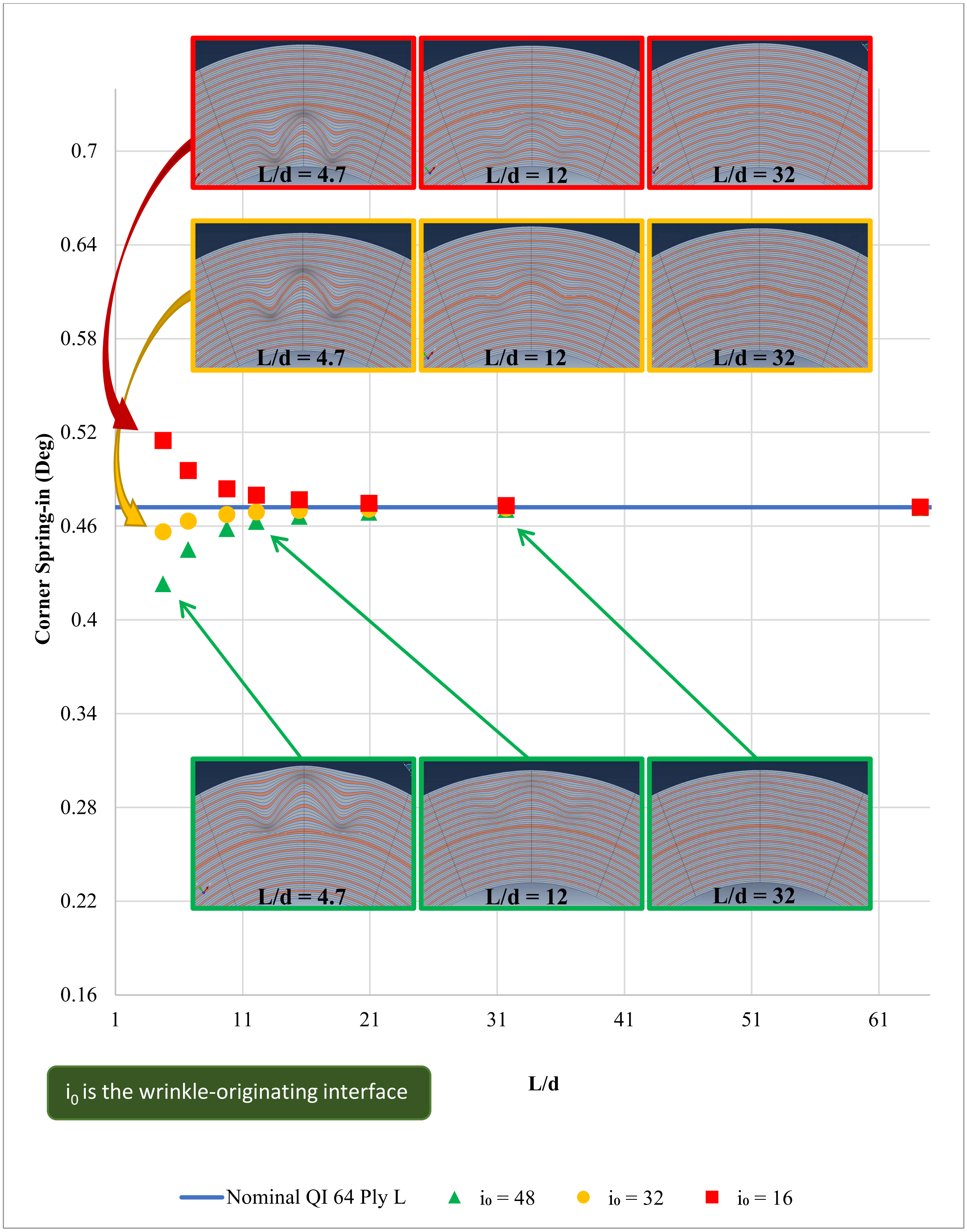

Figure 9. Effect of wrinkle-originating interface for narrow through-thickness attenuation, α_k = 10.

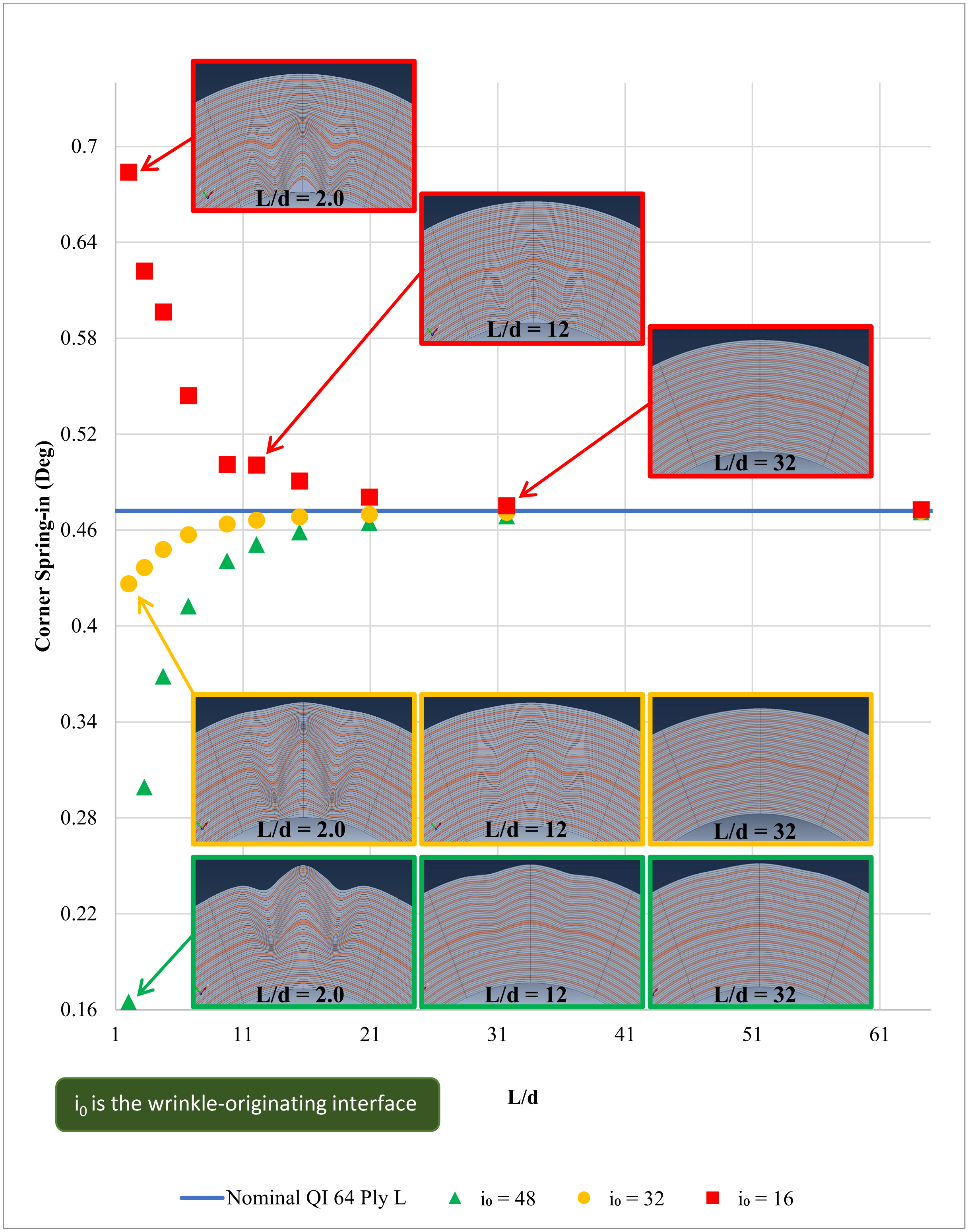

Figure 10. Effect of wrinkle-originating interface for moderate through-thickness attenuation, α_k = 20.

4.3. Interpretation, modelling limitations, and future work

With prescribed wrinkles, the local ply thickness changes while the assigned ply properties remain constant, so the model isolates geometric effects and does not capture property variations due to resin bleed, resin-rich/poor zones, or fibre volume-fraction changes. Wrinkles, therefore, modify the local thermal free-strain and stiffness distributions, which in turn alter the global corner spring-in.

This study is a controlled, constant-property cooldown sensitivity analysis: it does not model modulus evolution, cure shrinkage, wrinkle formation, resin flow, or fibre-volume-fraction-dependent properties. The spring-in decrease predicted for the midplane-originating wrinkle is not yet fully explained by the present model; initial hypotheses include geometric asymmetry due to the forced-smooth IML and fibre-rotation effects that alter the effective directional CTEs.

The methodology from this work can be incorporated into process-induced deformation models during product development to define allowable wrinkle limits. It can also support in-production assessments of the impact of wrinkles on dimensional tolerance, even when strength knockdown is acceptable.

Future work will introduce resin redistribution and volume-fraction effects. Extending the model to 3D and incorporating cure-dependent modulus and shrinkage using commercial process simulation software to capture coupled manufacturing physics throughout the full process history.

5. Conclusions

This work developed an automated 2D FE workflow that prescribes cured-in wrinkle geometry to study thermoelastic spring-in and flange warpage as an L-shape cools after cure. The results indicate that parameters such as wrinkle severity, through-thickness location, attenuation, repeated peaks, and flange propagation can affect the thermoelastic spring-in by up to 0.3°. Therefore, wrinkles should be considered not only as strength-knockdown defects but also as a factor for dimensional control. These results provide a basis for future defect-aware process-induced deformation modelling and for assessing the in-production impact of wrinkles on dimensional tolerance.

6. Acknowledgements

The authors would like to acknowledge the financial support of the industrial members of the Composites Research Network (The Boeing Company, Toray CMA, and Convergent) as well as the Canadian Federal Government (NSERC and PacifiCan) as well as many useful conversations with our industrial colleagues.

7. References

[1] CMH-17. *Composite Materials Handbook—17, Volume 3: Polymer Matrix Composites: Materials Usage, Design and Analysis*. Revision H, R-640, SAE International, Ch. 5, Sec. 11, 2025.

[2] D. W. Radford and T. S. Rennick. "Separating sources of manufacturing distortion in laminated composites". Journal of Reinforced Plastics and Composites, Vol. 19, No. 8, pp. 621-641, 2000.

[3] C. Netzel, A. Mordasini, J. Schubert, T. Allen, M. Battley, C. M. D. Hickey, P. Hubert and S. Bickerton. "An experimental study of defect evolution in corners by autoclave processing of prepreg material". Composites Part A: Applied Science and Manufacturing, Vol. 144, paper 106348, 2021.

[4] S. Mukhopadhyay, M. I. Jones and S. R. Hallett. "Compressive failure of laminates containing an embedded wrinkle: Experimental and numerical study". Composites Part A: Applied Science and Manufacturing, Vol. 73, pp. 132-142, 2015.

[5] N. Xie, R. A. Smith, S. Mukhopadhyay and S. R. Hallett. "A numerical study on the influence of composite wrinkle defect geometry on compressive strength". Materials & Design, Vol. 140, pp. 7-20, 2018.

[6] X. Xu, M. I. Jones, H. Ali, M. R. Wisnom and S. R. Hallett. "Effect of out-of-plane wrinkles in curved multi-directional carbon/epoxy laminates". Composites Science and Technology, Vol. 197, paper 108282, 2020.

[7] K. Çınar and N. Ersoy. "Effect of fibre wrinkling to the spring-in behaviour of L-shaped composite materials". Composites Part A: Applied Science and Manufacturing, Vol. 69, pp. 105-114, 2015.

[8] Y. Tao. "Process induced deformation of composite materials: An experimental methodology, systematic review and meta-analysis". M.A.Sc. thesis, The University of British Columbia, Vancouver, Canada, 2021.